


RESEARCH ARTICLE

Open Access



The 2016 M_w 5.9 earthquake off the southeastern coast of Mie Prefecture as an indicator of preparatory processes of the next Nankai Trough megathrust earthquake

Masaru Nakano^{1*} , Mamoru Hyodo¹, Ayako Nakanishi¹, Mikiya Yamashita¹, Takane Hori¹, Shin-ichiro Kamiya¹, Kensuke Suzuki¹, Takashi Tonegawa¹, Shuichi Kodaira¹, Narumi Takahashi^{1,2} and Yoshiyuki Kaneda^{1,3}

Abstract

Megathrust earthquakes have occurred repeatedly at intervals of 100 to 150 years along the Nankai Trough, situated in the southwest of Japan. Given that it has been 70 years since the last event, the occurrence of the next devastating earthquake is anticipated in the near future. On April 1, 2016, a moderate earthquake (M_w 5.9, M_{JMA} 6.5) occurred off the southeastern coast of Mie Prefecture in the source region of the 1944 Tonankai earthquake (M_w 8.2). In this study, we investigated the influence of the 2016 earthquake on future megathrust earthquakes. We first determined the hypocenter distributions using a precise velocity structure obtained from seismic surveys in the source region. Using data obtained from the DONET ocean-bottom observation network, we found that this earthquake occurred along the plate boundary fault, which is also believed to have slipped during past megathrust earthquakes. We then performed a preliminary numerical simulation to reproduce the occurrence of a moderate earthquake in the middle of a megathrust earthquake cycle. We used a hierarchical asperity model, in which smaller asperities causing moderate earthquakes are embedded in a hyper-asperity that serves as the source region of megathrust earthquakes. The simulation shows that moderate earthquakes, caused by ruptures of a smaller asperity, occur as a result of shrinkage of strongly coupled areas in the hyper-asperity. This result is consistent with the observation that the hypocenter of the 2016 earthquake was located at the edge of a strongly coupled region along the plate boundary. The simulation also reproduced postseismic slip (afterslip/slow slip) along the plate boundary updip of the hyper-asperity, which is consistent with the observations of slow slip events and very-low-frequency earthquakes after the 2016 earthquake. Thus, the occurrence of the moderate earthquake offshore southeastern Mie Prefecture in the middle of the megathrust earthquake cycle implies that the shrinkage of the strongly coupled area along the plate boundary is occurring as a preparatory process for the next megathrust earthquake in the region.

Keywords: Hypocenter determination, Crustal structure, Ocean floor observations, Accretionary prism, Earthquake cycle simulation, Hierarchical asperity model

* Correspondence: mnakano@jamstec.go.jp

¹R&D Center for Earthquake and Tsunami, Japan Agency for Marine-Earth Science and Technology, Yokohama, Japan

Full list of author information is available at the end of the article

Introduction

At convergent plate boundaries, large earthquakes occur repeatedly with intervals of one to several hundred years. The Nankai Trough, where the Philippine Sea plate (PSP) subducts beneath the Amur plate (Bird 2003; DeMets et al. 2010), is one such region where megathrust earthquakes and tsunamis have occurred at intervals of 100 to 150 years (e.g., Ando 1975; Ishibashi 2004). The 1944 Tonankai (M_w 8.2; Ichinose et al. 2003) and 1946 Nankai (M_w 8.4; Murotani et al. 2015) earthquakes were two such devastating events, which ruptured the eastern and western segments of the trough, respectively (Fig. 1), causing severe damage in western and central Japan. Future earthquakes with matching intensities will almost certainly result in severe damage, given the strong ground motion and tsunamis likely to be associated with them. Recent studies have indicated that such megathrust earthquakes would also cause massive damage due to long-period ground motion in distant regions, including metropolitan Tokyo (e.g., Furumura et al. 2008).

In order to clarify the deformation process along the convergent margin and the potential for such disasters, interdisciplinary studies, including seismic surveys of subsurface structures, seismic monitoring, geodetic observations, and numerical simulations, have been conducted. A number of seismic surveys have investigated geophysical and geological structures in detail (e.g., Mochizuki et al. 1998; Nakanishi et al. 1998, 2008; Park and Kodaira 2012; Park et al. 2002, 2003, 2010; Kamei et al. 2012). One of the most remarkable structures in the accretionary prism along the Nankai Trough is the megasplay fault or the out-of-sequence thrust branching from the decollement, imaged as strong reflections in multi-channel seismic survey (MCS) profiles (Park et al. 2002; Moore et al. 2007). Recent studies, based on detailed seismic surveys, have interpreted the megasplay fault as the main plate boundary fault (Bangs et al. 2009; Kamei et al. 2012, 2013; Tobin et al. 2014; Tsuji et al. 2014). The megasplay fault branches in the shallower part; one section reaches the ocean bottom and the other connects to the decollement beneath the toe of the accretionary prism (Tsuji et al. 2014). Both branches are considered to have slipped during past megathrust earthquakes (Sakaguchi et al. 2011; Tsuji et al. 2014).

Extensive observations of seismic activities along the Nankai Trough have been conducted using temporary deployments of recoverable ocean-bottom seismometers (OBS) (e.g., Obana et al. 2004; Obana and Kodaira 2009; Mochizuki et al. 2010). The recent development of a permanent seafloor observation network called the Dense Oceanfloor Network System for Earthquakes and Tsunamis (DONET) (Fig. 1 and Additional file 1: Figure S1) has facilitated continuous monitoring of offshore

seismic activities (Kaneda et al. 2015; Kawaguchi et al. 2015). These observations revealed that, in recent years, earthquake activities along the Nankai Trough have mostly occurred in the oceanic crust or upper mantle of the subducting PSP (Obana et al. 2004, 2005; Obana and Kodaira 2009; Mochizuki et al. 2010; Akuhara et al. 2013; Nakano et al. 2013, 2014, 2015; Akuhara and Mochizuki 2014). The most recent notable events during this time have been the 2004 M_{JMA} 7.1, 7.4, and 6.5 earthquakes off the Kii Peninsula, which occurred in the subducting plate (e.g., Sakai et al. 2005; Seno 2005).

Significant improvements in supercomputers have facilitated intensive numerical simulations of megathrust earthquakes (e.g., Hori 2006; Kodaira et al. 2006; Hori et al. 2009; Hyodo and Hori 2013). These studies have mainly focused on reproducing the slip distributions, rupture segmentations, and recurrence intervals of historical earthquakes, based on realistic fault models and subduction zone structures obtained from seismic surveys. In contrast, simulations based on simplified fault models can provide us with insights into earthquake rupture patterns, cycles, and related phenomena such as slow slip events (SSEs) (e.g., Matsuzawa et al. 2010; Noda et al. 2013, 2014; Ariyoshi et al. 2014). Hori and Miyazaki (2011) simulated occurrences of $M7-8$ earthquakes during $M9$ earthquake cycles to reproduce the occurrence of the 1978 M_w 7.5 earthquake that occurred offshore Miyagi before the 2011 Tohoku-oki earthquake (M_w 9.0). They used the hierarchical asperity model, in which a smaller asperity causing $M7-8$ earthquakes was embedded in a hyper-asperity that caused the $M9$ earthquake; namely, the fundamental rupture mode in the subduction zone. Numerical simulations can also indicate the temporal evolution of coupling ratios and stress states along fault interfaces. These parameters are, however, still very difficult to estimate from observations but are considered to be crucial for monitoring the preparatory processes of megathrust earthquakes (e.g., Kodaira et al. 2006). Thus, combinations of numerical simulations with seismic and geodetic observations could provide information about the current state of stress and strain along plate boundary faults.

On April 1, 2016, an earthquake occurred off the southeastern coast of Mie Prefecture ($M_w = 5.9$ as per the U.S. Geological Survey) (“off-Mie earthquake” hereafter). It occurred updip of the hypocenter of the 1944 Tonankai earthquake (Fig. 1a). The hypocenter was beneath the DONET stations, and real-time ocean-bottom observations were obtained. The epicenter was within the slip area of the 1944 Tonankai earthquake (Ichinose et al. 2003) and close to the eastern margin of the 1946 Nankai earthquake slip area (Murotani et al. 2015). During the 70-year period since the occurrence of the last megathrust earthquake, earthquakes with magnitudes

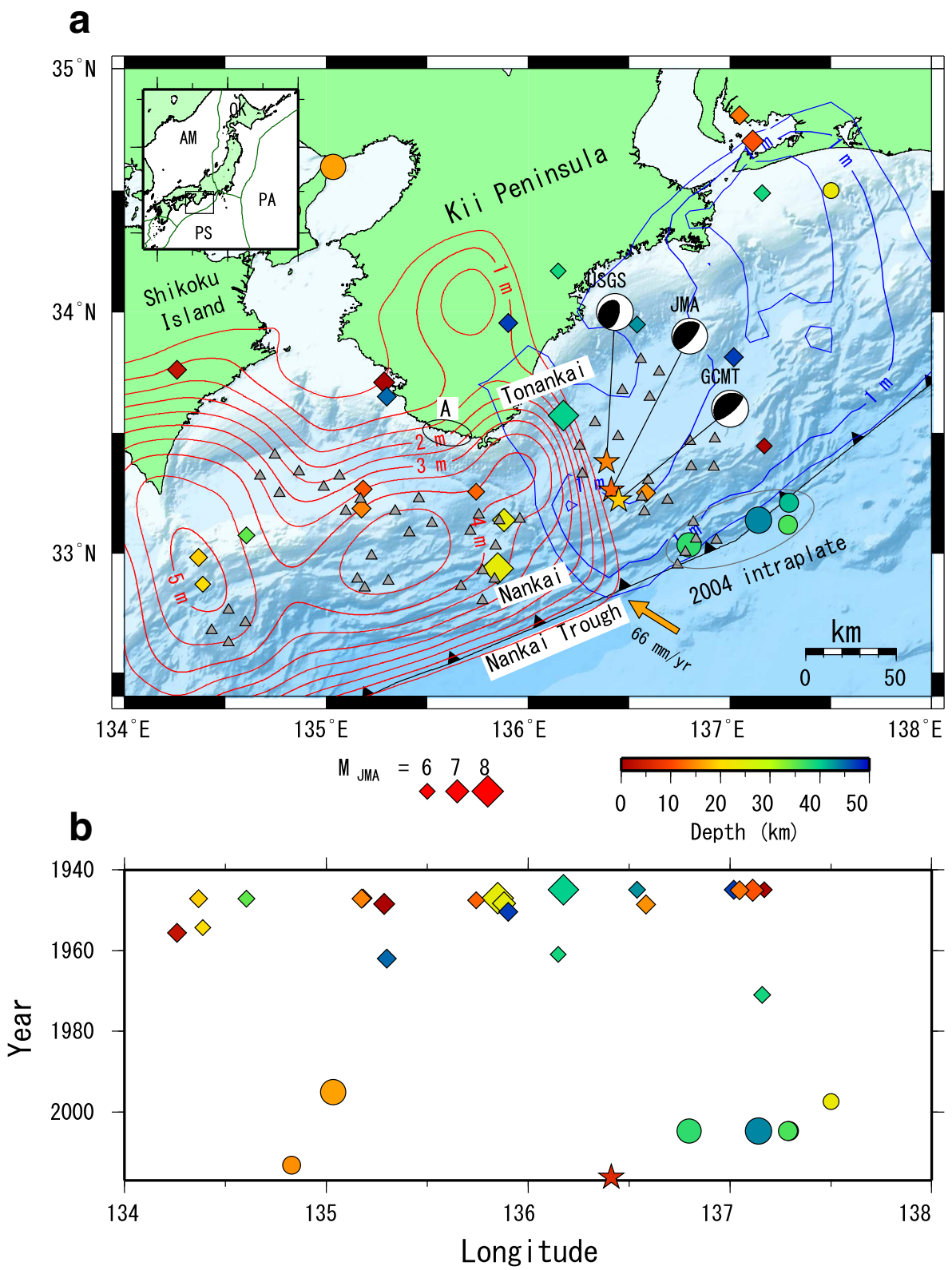


Fig. 1 (See legend on next page.)

(See figure on previous page.)

Fig. 1 Past seismic activities in the study area. **a** Regional location map (inset) and seismic activity along the Nankai Trough. Orange star represents the epicenter location of the 2016 off-Mie earthquake; results from the Japan Meteorological Agency (JMA), U.S. Geological Survey (USGS), and the Global CMT Project (GCMT) are shown together with mechanism symbols. Epicenters of earthquakes larger than M6 before and after 1976 are represented by diamonds and circles, respectively, from the JMA unified earthquake catalogue. Blue and red contours represent the slip distributions of the 1944 Tonankai and 1946 Nankai earthquakes, respectively (Ichinose et al. 2003; Murotani et al. 2015). Gray triangles represent locations of DONET stations. The ellipsoid labeled with “A” designates the region of interplate seismic activity reported by Akuhara and Mochizuki (2014). Orange arrows represent the subduction direction of the Philippine Sea plate. Plate name abbreviations are as follows: AM, Amur; OK, Okhotsk; PA, Pacific; PS, Philippine Sea. **b** Occurrence date of earthquakes plotted against their source longitude. Symbols are the same as in **a**

larger than 6 have been very rare along the eastern Nankai Trough (Fig. 1b). Exceptions were aftershocks of the 1944 and 1946 earthquakes that continued for about 10–15 years and the sequence of the 2004 intraplate earthquakes off the Kii Peninsula. Hence, large interplate earthquakes have not been known to occur until the middle of a megathrust earthquake cycle. Wallace et al. (2016) consider that the 2016 off-Mie earthquake most likely occurred on the plate interface, based on integrated analyses of hypocenter distributions, seafloor crustal deformations, and tsunami modeling using seafloor geodetic and seismological data from DONET. After this earthquake, SSEs along the plate boundary, very-low-frequency earthquakes (VLFs), and tectonic tremors have been observed updip of the hypocentral region (Fig. 2) (Annoura et al. 2017; Araki et al. 2017; Kaneko et al. 2018; Nakano et al. 2018). Recent studies have shown that signals from these slow events radiated from a common source (Kaneko et al. 2018; Nakano et al. 2018). The development of a comprehensive model of earthquake sources that can explain the generation of these regular and slow earthquakes would help us to understand the processes of stress accumulation and/or release along the plate boundary. It is important to determine the precise source location of the 2016 off-Mie earthquake to evaluate its influence on the generation of the next megathrust earthquake and its preparatory processes.

The centroid moment tensor (CMT) solution for the mainshock shows a thrust-type mechanism consistent with plate boundary slip (Fig. 1a). However, the source centroid location, which is based on regional or teleseismic data, is uncertain; depending on the institution that determined the location (Japan Meteorological Agency, U.S. Geological Survey, and the GlobalCMT project), there is a variation of ~20 km in the horizontal direction and 7 km (between 12 and 19 km) in depth. Such a discrepancy may have occurred because of strong structural heterogeneities that exist in the dip direction of plate subduction. Precise determination of the source location, especially for the depth, is crucial to clarify whether this earthquake occurred along the plate boundary. Wallace et al. (2016) determined the hypocenter distribution using a 1D velocity structure, which showed

that the sources were distributed very close to the plate interface. However, strong horizontal heterogeneities of seismic wave velocities due to plate subduction could affect the precision of determining the hypocenter locations. Takemura et al. (2016) showed that an accurate 3D velocity model reflecting the plate subduction is necessary to explain the spatial distributions of P-wave first motion polarities observed for this earthquake. Therefore, a velocity model reflecting the horizontal heterogeneities is crucial for precise determination of hypocenters.

In this study, we determined the hypocenters of the 2016 off-Mie earthquake and its aftershocks using a velocity model that includes horizontal heterogeneities along the subduction zone. We used a velocity structure obtained from a wide-angle OBS survey along a line passing through the source region shown by Wallace et al. (2016). We compared the hypocenter distribution with the MCS reflection profiles to confirm whether this earthquake occurred on the plate boundary. Since this earthquake was located along the plate boundary fault, we conducted a preliminary numerical simulation of plate boundary earthquakes to understand the implications of this earthquake for the Nankai Trough megathrust earthquake cycle. Using the hierarchical asperity model, we found that the 2016 off-Mie earthquake occurred due to shrinkage of the strongly coupled area along the plate interface, which is likely to be a preparatory process for the next megathrust earthquake. Interestingly, this model can also explain the absence of large earthquakes until the middle of the megathrust earthquake cycle.

Results and discussion

Hypocenter distribution of the 2016 off-Mie earthquake and aftershocks

We determined the hypocenters of the mainshock and aftershocks of the 2016 off-Mie earthquake using a local velocity model obtained in the source region (Fig. 2). We used a horizontally heterogeneous velocity structure based on that obtained along a survey line that passes through the hypocentral region (see the section “Methods/experimental”). The hypocenters were distributed several kilometers shallower than those based on

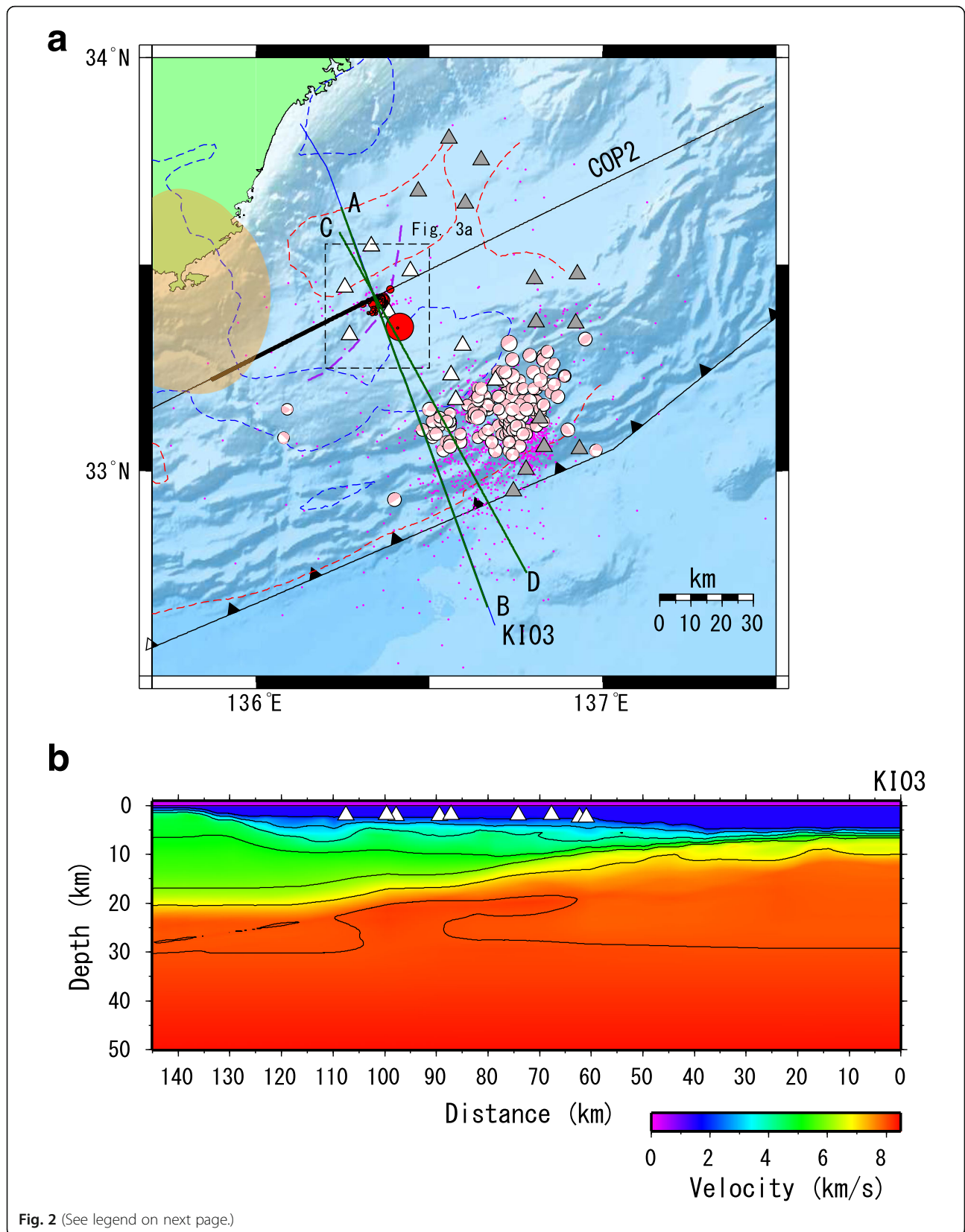


Fig. 2 (See legend on next page.)

(See figure on previous page.)

Fig. 2 Hypocenters of the off-Mie earthquake and aftershocks. **a** Hypocenter distribution of the 2016 off-Mie earthquake and aftershocks (red circles). Pink focal mechanism symbols indicate shallow VLFs, and magenta dots are locations of tectonic tremors in April 2016 (Kaneko et al. 2018; Nakano et al. 2018). White triangles represent DONET stations used for our hypocenter relocation. Green and blue lines represent location of MCS survey lines shown in Fig. 5. The thin black line represents the location of MCS survey line (COP2), and the thick black segment represents the location of a topographic high (Tsuru et al. 2005). The purple dashed line indicates the boundary of the topographic high in the basin. Red and blue dashed contours represent regions of low- and high-velocity anomalies, respectively, in the overriding plate (Yamamoto et al. 2017). A high-velocity body off the Kii Peninsula is represented by an orange oval (Kodaira et al. 2006). **b** Velocity structure used for our hypocenter determination obtained along MCS survey line K103 (Wallace et al. 2016)

our routine hypocenter determinations using a 1D velocity structure (Fig. 3). The mainshock depth was 9.2 ± 0.6 km below sea level, about 4 km shallower than that obtained by the routine analysis, and about 2 km shallower than that obtained by Wallace et al. (2016). The differences can be attributed to the horizontal heterogeneities of the velocity structure considered in our analysis. Aftershocks were distributed in a very limited area, about 10 km downdip of the mainshock, at depths of between 10 and 14 km, with source location errors of 1.9 km in both horizontal and depth directions. There is a seismic gap distinct from the mainshock hypocenter, which agrees with the results obtained by Wallace et al. (2016). The aftershock activity continued for 2 weeks, and a burst of reactivation occurred on April 19 (Fig. 4), coinciding with the end of the SSE following the mainshock (Araki et al. 2017).

The aftershock distribution can be further separated into two clusters: northeastern and southwestern (Fig. 3a). Events in the northeastern cluster were distributed almost parallel to the strike of the PSP, with a near-identical source depth, while those in the southwestern cluster showed a rather scattered distribution in the dip direction. Event sizes were systematically larger in the northeastern cluster, and decay times of these activities were clearly different. Activity in the northeastern cluster lasted for only a day, whereas, in the southwestern cluster, it continued for much longer (Fig. 4).

Figure 5 compares the earthquake depths and reflectors imaged from MCS surveys along lines passing through the source region (see the section “Methods/experimental”). Clear reflections indicative of the plate boundary are observed in the MCS profiles. The mainshock was located at a slightly shallower depth than the upper reflector, possibly corresponding to the megasplay fault. The aftershocks were distributed about 10 km landward from the mainshock, at depths about 2 km deeper than the reflector (Fig. 3). This result agrees with that of Wallace et al. (2016), although the separation depth was comparable to the location errors.

Considering the location errors associated with determining the hypocenters and reflector depths (± 1.1 km), we consider that this earthquake has slipped along the plate boundary fault, as Wallace et al. (2016) reported,

but the depth difference from the plate boundary fault was smaller in our result. The hypocenter location corresponds to the shallower edge of the strongly coupled region along the plate boundary, as noted by Yokota et al. (2016) (Additional file 2: Figure S2).

Earthquake cycle simulation based on the hierarchical asperity model

In order to investigate the generating mechanism of the off-Mie earthquake in the middle of the megathrust earthquake cycle along the Nankai Trough, we conducted a preliminary earthquake cycle simulation based on the hierarchical asperity model (Hori and Miyazaki 2010, 2011) that has been used previously to simulate multiscale earthquakes. In this model, smaller asperities, causing moderate-sized earthquakes, are embedded in a larger asperity (“hyper-asperity”), causing the fundamental rupture mode of the fault system. To simulate the generation of earthquakes on a megathrust, we solved the quasi-dynamic equation of shear stress along fault segments (Rice 1993) using the rate- and state-dependent friction (RSF) laws to represent frictional properties across the fault (see the section titled “Methods/experimental”). The occurrence of an earthquake on the plate boundary is modeled as a perturbation from the steady-state relative plate motion. Shear stress builds up due to secular motion of the subducting plate which is finally released as earthquakes when the accumulated shear stress exceeds the fault strength governed by RSF.

In our simulation, we attempted to reproduce the following characteristics observed for the off-Mie earthquake. First, the earthquake occurred after 70 years of a quiet period characterized by the absence of M6 or larger earthquakes after the previous M8 earthquake. Second, a slow slip and/or afterslip episode was observed immediately after this earthquake (Wallace et al. 2016; Araki et al. 2017). In order to reproduce such complicated slip behavior during an earthquake cycle, we need to properly define the frictional parameters along the megathrust, as well as the sizes and locations of asperities. Suitable parameters need to be determined empirically and the computational cost for conventional 3D simulations is high; hence, we conducted 2D simulations

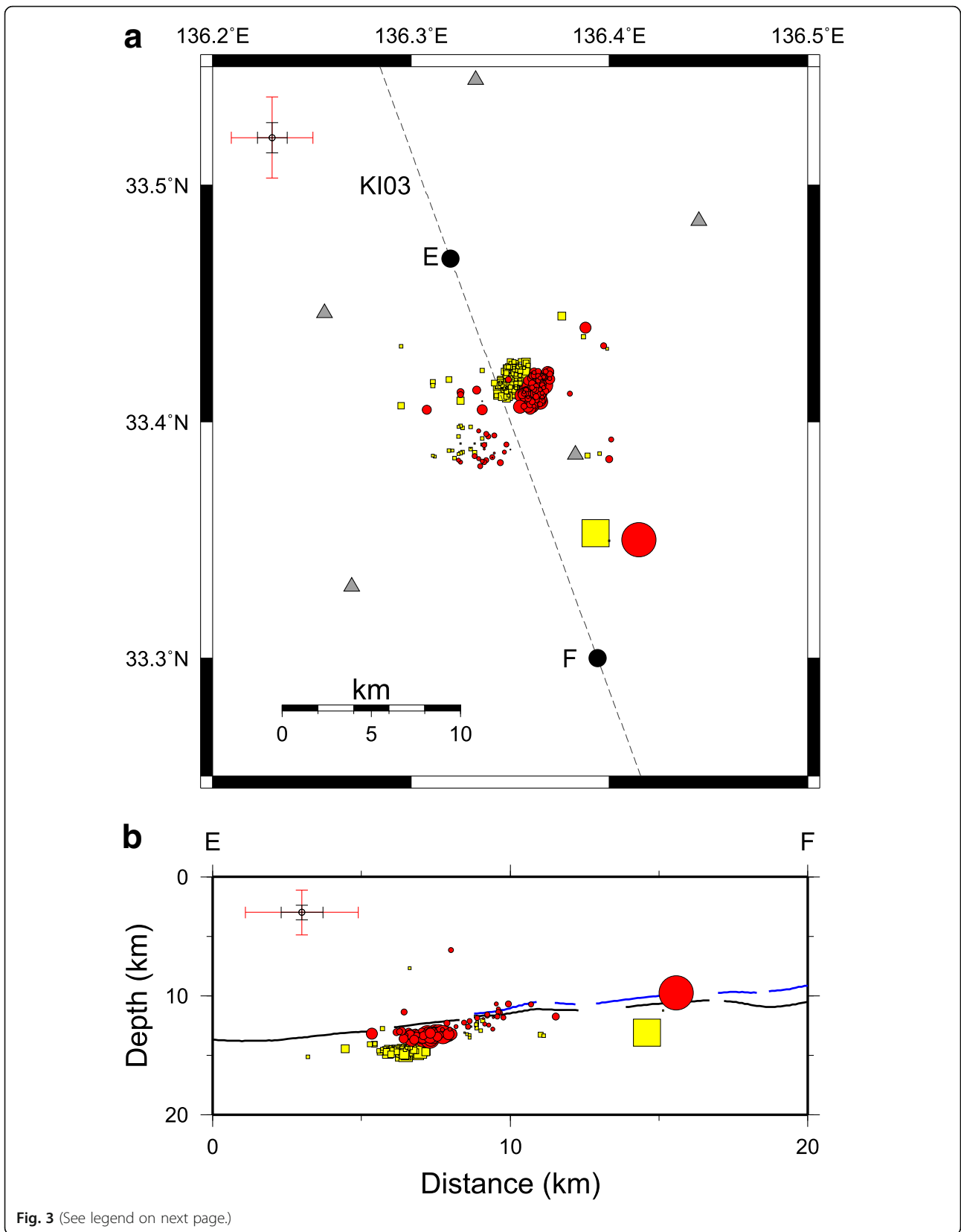


Fig. 3 (See legend on next page.)

(See figure on previous page.)

Fig. 3 Comparison of routine and relocated hypocenter locations. Yellow and red circles represent routine and relocated hypocenters, respectively. Black and red crosses at the top left of each panel represent the uncertainties of hypocenter locations for the mainshock and aftershocks, respectively. **a** Map view. Gray triangles represent locations of DONET stations. **b** Cross-section along line E–F. Black and blue lines represent strong reflections picked from the MCS profile shown in Fig. 5a

(temporal evolution of slip on a fault, represented by line segments) for the parameter search. In this study, we present one of the simulation results that reproduced the characteristics described above well.

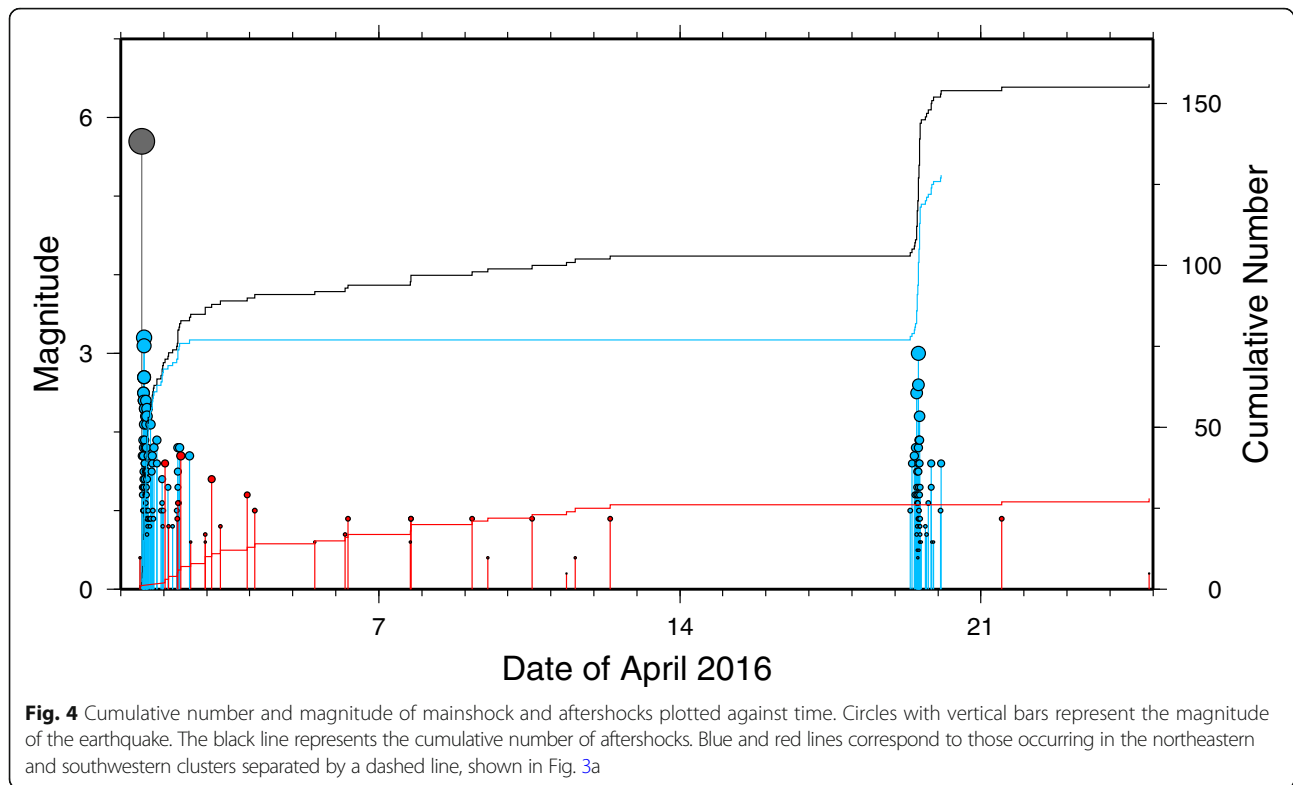
In the numerical simulation, the frictional parameters of asperities are set as unstable slip conditions, while regions outside of them are set as stable. Since the hypocenter of the off-Mie earthquake was located at the shallower edge of the strongly coupled region along the Nankai Trough (Additional file 2: Figure S2), we defined a smaller asperity, causing an M6-class earthquake, at the shallower edge of the hyper-asperity. Figure 6 shows the fault geometry and frictional parameters, in which we assume two smaller asperities (dark blue segments) embedded in the hyper-asperity (both dark blue and light-blue segments). Based on a simulation using this frictional parameter distribution, the rupture of a shallower asperity placed on a 10-km-long line segment along the plate boundary fault, corresponding to a 10–11 km depth range (“shallower asperity” hereafter), caused the M6 earthquake. Whereas, the rupture of a deeper asperity, a 30-km-long segment along the plate boundary fault corresponding to a 13–17 km depth range (“deeper asperity” hereafter), propagates along the entire hyper-asperity to cause an M8 earthquake, the fundamental rupture mode of this fault system.

Figure 7a shows the spatiotemporal evolution of the slip rate along the fault. At the beginning of the M8 megathrust earthquake cycle (marked by “M8” at the bottom of Fig. 7a), the slip velocity on the fault is very small along the entire asperity, that is, the fault is strongly coupled. Outside the hyper-asperity, a secular aseismic slip occurs during the entire earthquake cycle because of the stable sliding frictional properties. The strongly coupled area on the hyper-asperity gradually shrinks from the deeper and shallower edges due to the secular aseismic slip, which causes a gradual increase in shear stress on the shallower and deeper asperities (Fig. 8). From the first half to the middle stage of the M8 megathrust earthquake cycle, the rate of increase of stress is higher in the shallower asperity because of its location closer to the edge of the hyper-asperity. In our simulation, it takes about 120 years for sufficient stress to accumulate to rupture the shallower asperity (M6 earthquake) in a 200-year megathrust earthquake cycle. The M6 earthquake is followed by postseismic slip (afterslip/slow slip) that occurs mainly in a region of velocity-strengthening frictional parameters, that is, an

updip of the hyper-asperity, and continues for more than 20 days (Fig. 7b). After the occurrence of the M6 event, the strongly coupled area in the hyper-asperity further shrinks because of the secular aseismic slip in the surrounding area, and the shear stress of the deeper asperity further increases (Fig. 8). When the stress at the deeper asperity reaches the threshold, a rupture initiated at the asperity propagates along the entire hyper-asperity and an M8 earthquake occurs.

Using earthquake cycle simulation based on the hierarchical asperity model, we successfully reproduced the occurrence of a moderate earthquake in the middle of the megathrust earthquake cycle and the SSE (or afterslip) that follows the earthquake. The rupture of the shallower asperity is caused by shrinkage of the strongly coupled area along the hyper-asperity, which results from the secular plate subduction. This finding implies that the occurrence of the moderate 2016 off-Mie earthquake in the middle of the earthquake cycle represents shrinkage of a strongly coupled area, which could be a preparatory process of the next megathrust earthquake along the Nankai Trough. We note here that the cycle of the M8 earthquake and the timing and frequency of the M6 earthquake depend on the frictional parameters of the fault, their distributions, and the slip velocity at the plate interface, all of which were assumed in the simulation.

Aftershocks of the off-Mie earthquake occurred only downdip of the mainshock, with a clear separation of about 10 km (similar to Wallace et al. 2016). The absence of an updip aftershock is not surprising, because this region is considered to have conditionally stable frictional properties (Wallace et al. 2016). Instead, slow earthquakes as SSEs, VLFES, and tectonic tremors occurred there, sharing a common updip source region (Araki et al. 2017; Kaneko et al. 2018; Nakano et al. 2018) (Fig. 2). Both regular and slow earthquakes were almost entirely absent between the downdip aftershocks and updip slow earthquakes, although the occurrence of an SSE or an afterslip close to the hypocenter region was implied after the mainshock (Wallace et al. 2016; Nakano et al. 2018). Our numerical simulation successfully reproduced the slow slip updip of the asperity, where stable sliding frictional parameters were defined. Although the reason for the existence of a gap between the mainshock hypocenter and aftershocks is still elusive, Tsuji et al. (2017) considered that aftershocks occurred close to the location where the plate boundary



decollement soles out into the top of oceanic crust layer 2 (TOC). Such heterogeneous structures may cause stress accumulations, which could explain the very limited aftershock distribution. Wallace et al. (2016) suggested that this gap coincided with the mainshock fault that did not trigger aftershocks because stress was already released, or stress was released due to aseismic slow slip, or both. The migration of VLFE sources updip, away from the mainshock hypocenter, supports the latter model (Nakano et al. 2018).

The aftershock activity was separated into two clusters, which showed different decay times, namely, the p value of the Omori–Utsu aftershock decay law (Figs. 3 and 4). The Omori–Utsu law is given as $n(t) = K(t + c)^{-p}$, where $n(t)$ is the number of events per unit time at t since the mainshock; K , c , and p are constants (Utsu 1961). Although source properties corresponding to the p value are not well studied, Kisslinger and Jones (1991) observed that high heat flow causes a high p value. They considered that the p value represents the stress relaxation time, and the aftershock decay rate is controlled by the temperature at the source depth. In our case, however, the distance of the aftershock clusters was only several kilometers and the temperature would not differ significantly. Mikumo and Miyatake (1979) conducted numerical simulations and showed that the p value becomes smaller as the distribution of fault strength becomes more heterogeneous. Small-scale heterogeneities

in geological structures would cause differences in frictional properties along aftershock faults. The aftershock region corresponds to the boundary between older (~14 Ma) and younger (~6 Ma) prisms (Tsuji et al. 2017), which would lead to a difference in the degree of heterogeneities in plate boundary structure.

Previous studies showed that structural heterogeneities exist in overriding and subducting plates around the source region of the off-Mie earthquake (Fig. 2). One of the characteristic structures off the Kii Peninsula is a plutonic rock body with high seismic velocity and high density, which is coincident with the segment boundary of megathrust earthquakes along the Nankai Trough (Kodaira et al. 2006). A topographic high in the TOC can be recognized to the west of the aftershock area in the MCS reflection survey obtained along the strike direction of the subducting plate (line COP2 in Tsuru et al. (2005)). A boundary of the ocean floor topography (the purple dashed line in Fig. 2a) is also coincident with the epicenter distribution of the aftershocks. This region corresponds to the boundary of low- and high- velocity anomalies in the overriding plate (Yamamoto et al. 2017). The source of the off-Mie earthquake is close to the boundary of the backstop and sediments (Tsuji et al. 2015) and also corresponds to the location where the decollement soles out into the TOC (Tsuji et al. 2017). Tsuji et al. (2017) also pointed out that the aftershock region corresponds to the boundary between the older

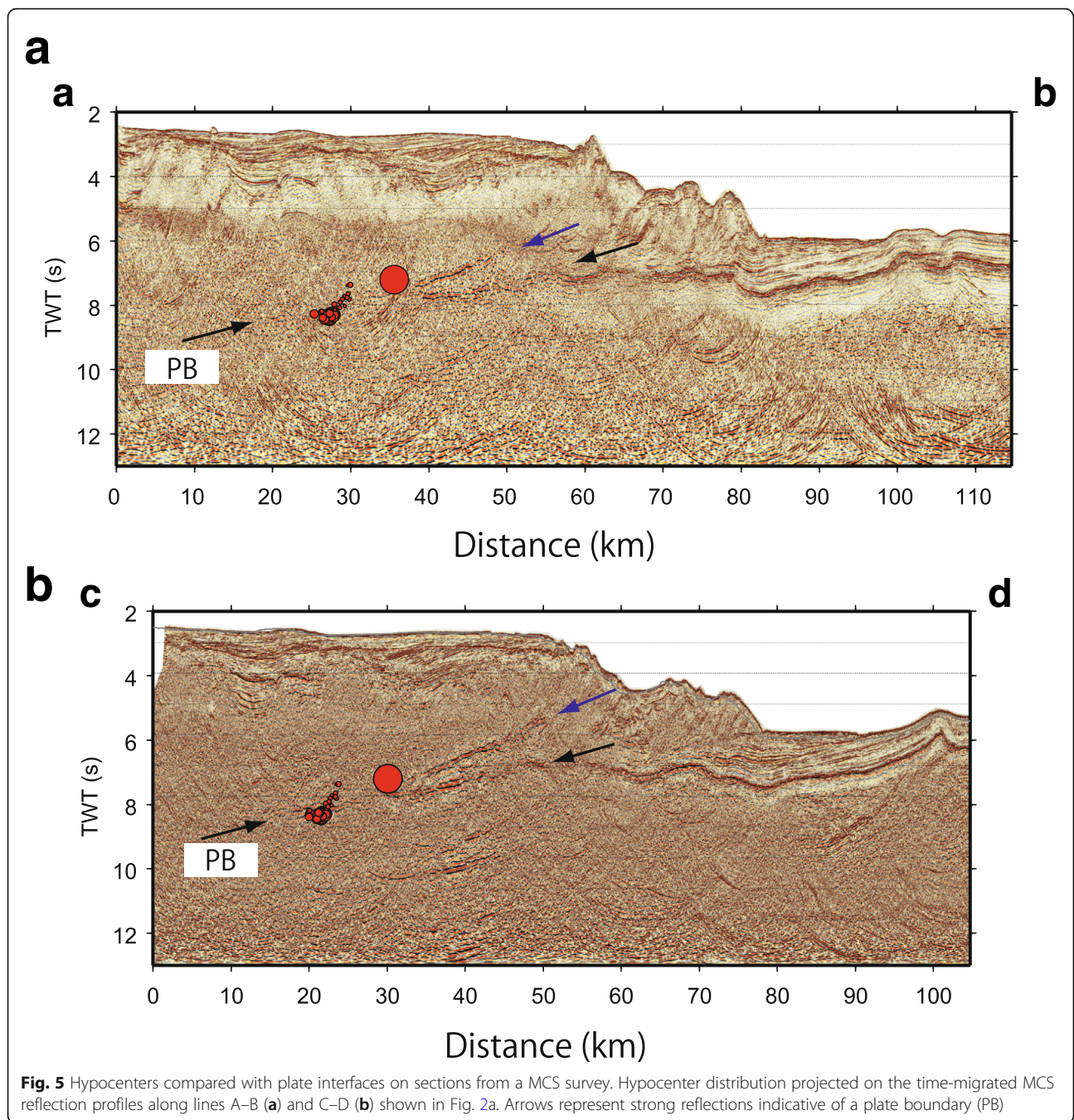
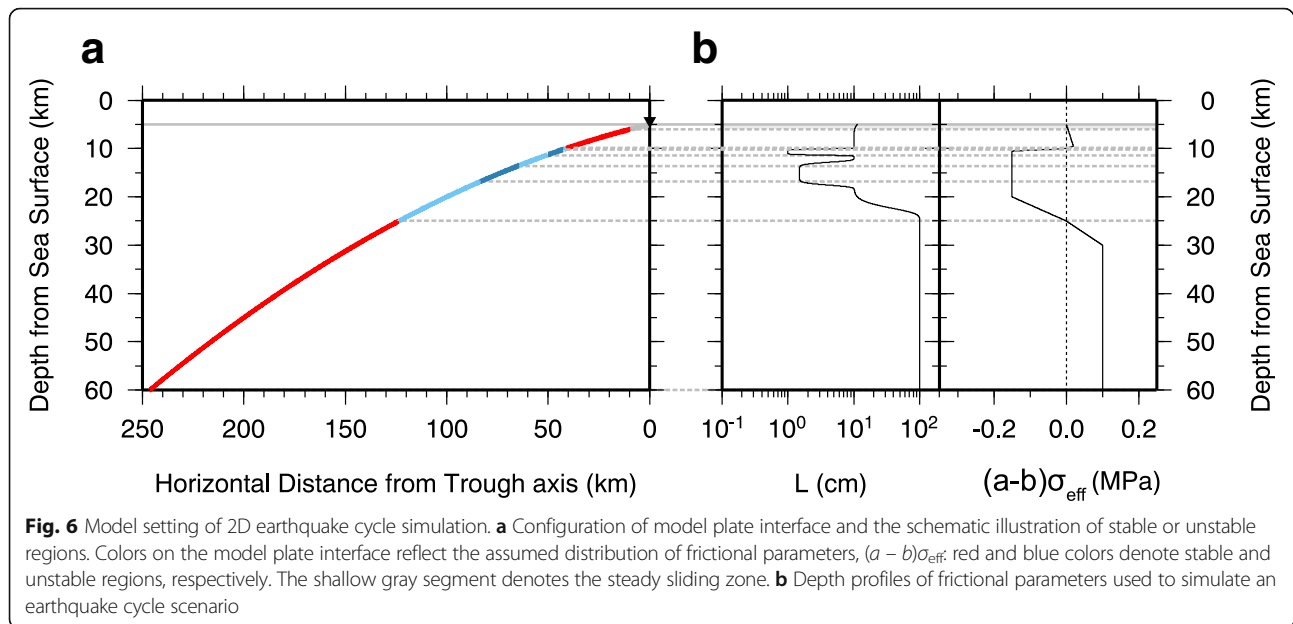


Fig. 5 Hypocenters compared with plate interfaces on sections from a MCS survey. Hypocenter distribution projected on the time-migrated MCS reflection profiles along lines A–B (a) and C–D (b) shown in Fig. 2a. Arrows represent strong reflections indicative of a plate boundary (PB)

and younger prisms. These heterogeneous structures concentrate stress and limit the area of the aftershock activity.

In our earthquake cycle simulations, we successfully reproduced the occurrence of a moderate earthquake in the middle of the megathrust earthquake cycle. The simulation implies that the M6-class off-Mie earthquake was caused by shrinkage of the strongly coupled area along the plate boundary. Present seismic activities in the eastern Nankai Trough are mostly within the

subducting or overriding plates, and there is very low activity in the rupture area of the megathrust earthquakes (Obana et al. 2004; Obana and Kodaira 2009; Nakano et al. 2015). However, Akuhara and Mochizuki (2014) observed continuous activity of an earthquake cluster with magnitudes smaller than 4 along the plate boundary west of the Kii Peninsula (labeled “A” in Fig. 1a). Their hypocenters roughly correspond to the downdip end of the rupture area of the 1946 Nankai earthquake (Murotani et al. 2015). These observations imply that the



asperity of the earthquake cluster is continuously loaded because of weak interplate coupling, probably due to the shrinkage of the strongly coupled region. In fact, the slip deficit rate in this region is less than that in the source region of the off-Mie earthquake (Yokota et al. 2016). Monitoring such seismic activities based on precise hypocenters is important for the understanding of the state of interplate coupling along the plate boundary fault, as well as geodetic data inversion. To achieve this, a local 3D velocity structure is crucial for accurate hypocenter locations (Akuhara et al. 2013; Yamamoto et al. 2017).

If other asperities exist, their ruptures could occur in the middle of the megathrust earthquake cycle due to the decrease in the interplate coupling ratio (Hori and Miyazaki 2011). The timing and magnitude of the earthquake depends on both the location and size of the asperities. Our simulations can also model the magnitude, timing, frequency of the moderate earthquake, and the interval of the fundamental rupture mode causing the megathrust earthquake by defining the fault frictional parameters appropriately. In our 2D simulations, the moderate M6 earthquake occurs 120 years after the M8 earthquake, with a cycle of about 200 years. Both values are much longer than the observed values: the cycle of megathrust earthquakes in the Nankai Trough is considered to be 100 to 150 years (Ando 1975; Ishibashi 2004), and the off-Mie earthquake occurred 70 years after the previous 1944 Tonankai earthquake. In 3D simulations, however, these periods would become shorter with the same frictional parameter values because the shrinkage of the coupled area on the asperity also occurs in the strike direction of the fault. Studies based on more realistic fault geometry and frictional parameter

distributions on a 3D model would improve our understanding of earthquake cycles along plate boundaries.

Conclusions

Using a local velocity model, we found that the 2016 Mw5.9 earthquake off the southeastern coast of Mie Prefecture occurred on the plate boundary along the Nankai Trough. We performed a numerical simulation based on a hierarchical asperity model, which successfully reproduced the occurrence of a moderate earthquake in the middle of a megathrust earthquake cycle. The results of the numerical simulation imply that the occurrence of the off-Mie earthquake represents shrinkage of the interseismically coupled area along the plate boundary and serves as an indication of the preparatory processes of the next megathrust earthquake.

Methods/experimental

Hypocenter determinations using a 2.5-D velocity model

The strong heterogeneity in the seismic velocity structure in the subduction zone prevents precise hypocenter determinations. We used the 2-D velocity structure obtained from a tomographic inversion of the first-arrival refraction travel times of a wide-angle OBS survey along line KI03, which passes through the hypocenter region (Fig. 2) (Wallace et al. 2016). Using this 2D structure, we created a 3-D velocity volume, assuming that the structure is identical along the strike of the subducting plate; then, we computed theoretical travel times at each DONET station. Since the PSP strikes about 40° N around the hypocenter region (Citak et al. 2012) (Additional file 1: Figure S1), the 2D structure is oriented in this direction (Additional file 3: Figure S3). We

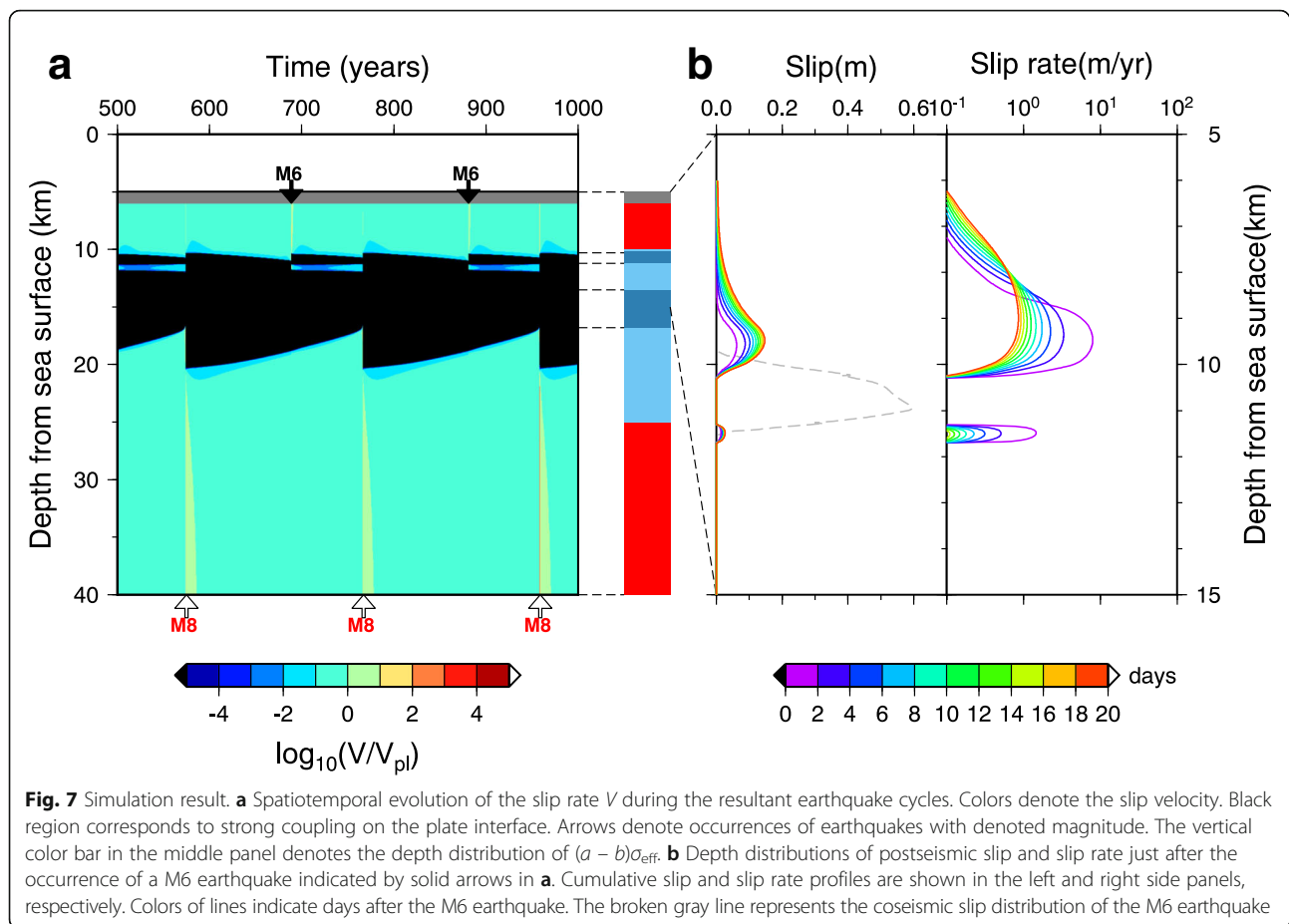


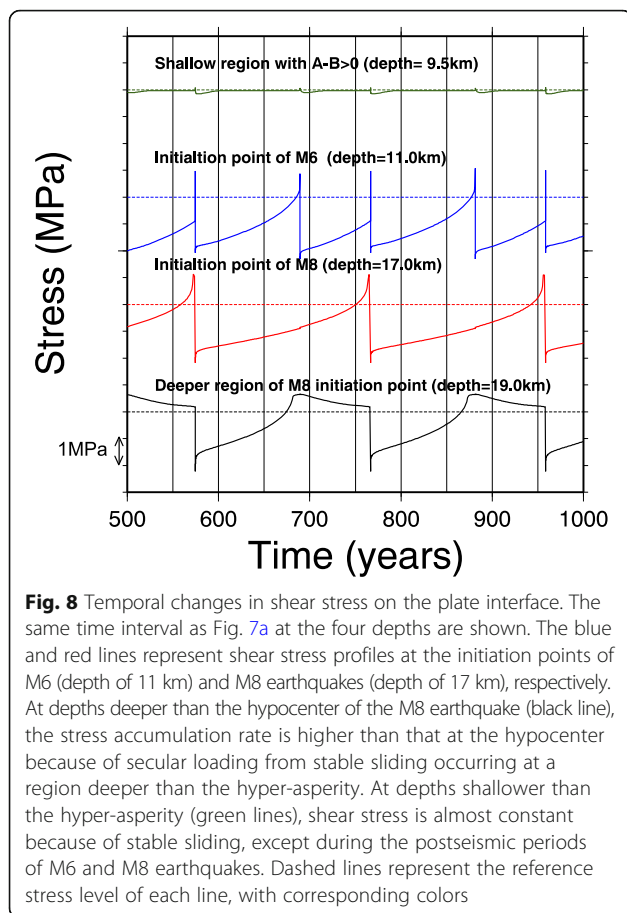
Fig. 7 Simulation result. **a** Spatiotemporal evolution of the slip rate V during the resultant earthquake cycles. Colors denote the slip velocity. Black region corresponds to strong coupling on the plate interface. Arrows denote occurrences of earthquakes with denoted magnitude. The vertical color bar in the middle panel denotes the depth distribution of $(a-b)\sigma_{eff}$. **b** Depth distributions of postseismic slip and slip rate just after the occurrence of a M_6 earthquake indicated by solid arrows in **a**. Cumulative slip and slip rate profiles are shown in the left and right side panels, respectively. Colors of lines indicate days after the M_6 earthquake. The broken gray line represents the coseismic slip distribution of the M_6 earthquake

call this the 2.5-D model for convenience because of the similarity to the computations of wave propagation in three dimensions using a 2-D velocity model (e.g., Takekawa and Kennet 1996). We did not use the model of Kamei et al. (2012) because it did not fully cover the study area.

For the hypocenter determinations, we used the seafloor seismic recordings from a broadband seismometer installed at each DONET station. We manually picked P-wave onsets from the vertical component seismograms. To avoid the effect of possible heterogeneities in the accretionary prism in the strike direction of the PSP, we only used data from nine stations located within 30 km of the mainshock source (white triangles in Fig. 2a). Moreover, we did not use S-wave arrival times because of the uncertainty in S-wave velocity, especially in the soft sediments covering the accretionary prism. We used NonLinLoc software (Lomax et al. 2000) for the hypocenter determinations. This software adopts the eikonal finite-difference scheme of Podvin and Lecomte (1991) to compute first-arrival times at each station in a 3D volume for hypocenter determinations using heterogeneous velocity structures. We estimated site corrections for the P-wave travel

time at each station by averaging the residuals between the theoretical and observed travel times and redetermined the hypocenter locations. This procedure was repeated three times to obtain the final solution. The resulting site corrections are within ± 0.09 s, except at KME19, which needed a correction of -0.17 s. The source location errors are 0.7 km in the horizontal direction and 0.6 km in the vertical direction for the mainshock and 1.9 km in both directions for the aftershocks. The root-mean-square (RMS) of travel time residual is 0.02 s.

We examined the accuracy of the hypocenter depths by changing the dataset or assumed strike of the PSP (see the Additional file 4: Supplementary note). Aftershock depths were several kilometers shallower when we included distant stations (Additional file 5: Figure S4). This difference could be caused by horizontal heterogeneities of the structure along strike (e.g., Park et al. 2010). The increasing RMS travel time residual, including distant stations, implies that theoretical travel times are less accurate at distant stations because of inaccurate velocity structures. Stable aftershock depths were obtained when using S-wave arrival times or changing the



strike of the PSP. Moreover, the mainshock depth was stably located for most cases. Consequently, we consider the obtained hypocenter locations to be stable.

We also computed hypocenters by our routine analysis based on a 1D velocity structure, using P- and S-wave readings from all DONET stations (Fig. 3). The mainshock hypocenter was located several kilometers east of the 3D result, at a depth of 13.1 km. Aftershocks were distributed several kilometers west of the 3D result, at a depth of about 15 km. We note that this computation is different from that of Wallace et al. (2016), which only uses P-wave readings from stations connected to nodes D and E.

Comparison of hypocenter depths with reflectors obtained from MCS profiles

We compared the hypocenter depths with distinct reflectors in the accretionary prism obtained from MCS reflection surveys (Fig. 5). We converted the hypocenter depths to two-way travel times (TWTs) by integrating the slowness from sea level to the hypocenter depth picked at the epicenter, based upon the velocity structure used for the hypocenter determinations (Fig. 2b). While the MCS profile shown in Fig. 5a was obtained

along the same line as the velocity structure, the profile in Fig. 5b was obtained along an intersecting line. Hence, the TWTs on this profile do not exactly match those computed from the hypocenter depths due to possible along strike heterogeneity of the subduction zone.

We picked TWTs of strong reflections indicative of the plate boundary from the MCS reflection profile (Fig. 5a), converted them to depth values by inverting the process described above, and plotted them on the depth section (Fig. 3b).

The uncertainties in picking the reflections are about 0.15 s, corresponding to 1.1 km at reflector depths. The errors in hypocenter depths correspond to a TWT error of 0.31 s for the mainshock and 0.67 s for the aftershocks.

Two-dimensional forward simulation of M8-class earthquake cycles along the Nankai Trough

Here, we attempt to interpret the conceptual relation between M8-class interplate earthquakes (such as the 1944 Tonankai earthquake) and the occurrence of a smaller earthquake (such as the 2016 off-Mie earthquake) inside the source region through seismic cycle modeling, which assumes the equilibrium of quasi-dynamic shear stresses on the fault and frictional resistance governed by a rate- and state-dependent friction (RSF) law.

Governing equations for quasi-dynamic seismic cycle simulation

In quasi-dynamic seismic cycle modeling, the occurrence of interplate earthquakes on plate boundaries has often been modeled as a perturbation from the steady-state relative plate motion by ignoring the contribution of steady (forward) slip on the whole plate interface. Thus, the interseismic process is expressed as the accumulation of slip deficit (or backslip) in the seismogenic zone. The shear stress builds up with time as the slip deficit increases, and the accumulated slip deficit is finally released as earthquakes when the accumulated shear stress exceeds the fault resistance governed by RSF. Below, we briefly describe equations governing the earthquake cycle simulation used here.

At first, by discretizing the target plate interface into N small sub-faults, we define physical variables associated with seismic cycles for each sub-fault: shear stress τ_i , state variable θ_i representing contact state, and slip velocity V_i . Here, subscript i specifies the particular sub-fault ($1 \leq i \leq N$). When the material containing the fault (or a set of sub-faults) is a linear-elastic one, temporal changes in shear stress can be approximated through the whole seismic cycle using the quasi-dynamic expression given by Rice (1993) as follows,

$$\frac{d\tau_i(t)}{dt} = - \sum_{j=1}^N K_{ij}(V_{pl}-V_j(t)) - \frac{G}{2V_s} \dot{V}_i(t), \quad (1)$$

where K_{ij} represents the static slip response function between sub-faults, and V_{pl} is the relative plate velocity of the target plate interface, assumed to be constant regardless of sub-faults. V_s and G represent shear-wave velocity and rigidity of the material containing the fault, respectively. The first term on the right-hand side in Eq. (1) denotes the contribution of slip deficit rate distribution to the change in shear stress. It should be noted that since only perturbation from the steady-state subduction is treated, shear stress of sub-fault i is designed so as not to be affected by sub-fault j if the j -th sub-fault is slipping with the same slip velocity as relative plate motion, V_{pl} . Further, because the static slip response function K_{ij} is used in the first term, the radiation damping term, representing the effect of wave propagation, is added as the second term to better approximate the stress state through the entire seismic cycle, including the coseismic stage.

As previously mentioned, we assume that fault friction governed by RSF resists fault motion during an earthquake cycle. The friction coefficient μ following RSF is generally defined as,

$$\mu_i(t) = \mu_* + a_i \ln \frac{V_i(t)}{V_*} + b_i \ln \frac{V_* \theta_i(t)}{L_i} \quad (2)$$

The first term μ_* is a reference friction coefficient at the steady-state sliding with the reference slip rate V_* , while the second and third terms of the right-hand side on Eq. (2) represent contributions of slip rate (i.e., V) and state variable (i.e., θ) to the friction coefficient, respectively. As the state variable θ is an indicator of the contact state at the fault interface, the third term represents the dependency of the frictional coefficient on “contact” state. Several versions have been proposed for the evolution of the state variable θ to describe state variable-dependency on μ . We adopt a widely used version, known as an “aging law”, given by,

$$\frac{d\theta_i(t)}{dt} = 1 - \frac{V_i(t)\theta_i(t)}{L_i} \quad (3)$$

In this study, we simply set $V_* = V_{pl}$. Parameters a , b , and L in Eqs. (2) and (3) are called frictional parameters. As shown in Eq. (2), a and b are parameters concerning rate- and state-dependencies of friction, respectively. L represents a characteristic slip distance necessary for the friction μ to decrease significantly. In other words, the lower the value of L assumed, the larger the decreasing

rate of friction for a particular slip amount. Because these parameters characterize the frictional property of the fault, and accordingly control the spatial and temporal behavior of fault slip, we must pay special attention to the distribution of the frictional parameters on the model fault in seismic cycle simulations.

The frictional stress on the plate interface is expressed as the product of the frictional coefficient μ and effective normal stress σ_{eff} . Changes in fault frictional stress ($d(\mu\sigma_{\text{eff}})/dt$) are assumed to balance changes in shear stress (Eq. (1)). We then obtain simultaneous differential equations with respect to V_i and θ_i for $0 \leq i \leq N$. Under the hypothetical distribution of frictional parameters a_i , b_i , and L_i for $0 \leq i \leq N$, we can simulate the spatiotemporal slip behavior on the target plate interface by integrating the simultaneous differential equations from a particular initial condition (and boundary condition if required).

Configuration of model plate interface and its discretization

In order to reproduce the complicated slip behavior during an earthquake cycle, we need to set appropriate frictional parameters along the megathrust. To obtain a suitable set of parameters, we require many computations with trial parameter settings. To reduce the computational cost for the seismic cycle simulation including multiple earthquakes with a larger gap in magnitudes compared with the previous studies (Hori and Miyazaki, 2010, 2011), we conducted 2D simulations instead of conventional 3D ones. In the 2D simulation, we modeled the plate boundary fault with a set of line segments, as the vertical cross section perpendicular to the Nankai Trough axis off the Kii Peninsula. The configuration of the upper interface of the subducting PSP was simply assumed to be a smooth curve with an average dip angle of about 12° (Fig. 6a). For this vertical cross section, we discretized the curved plate interface into 4400 line segments of nearly equal lengths of about 50 m. We confirmed that this length of line segment is sufficient to accurately model earthquake cycles with the distribution of frictional parameters shown later. Each line segment corresponds to a sub-fault; the slip response function K_{ij} for this type of sub-fault was calculated by the analytic expression given by Rani and Singh (1992), which determines the stress change under the plane strain field due to the unit dip slip of each sub-fault in an elastic half space consisting of a Poisson solid with $G = 30$ GPa and $V_s = 3273$ m/s. We assumed $V_{pl} = 5$ cm/year for the plate subduction velocity.

Distribution of frictional parameters

Colors on the model plate interface in Fig. 6a reflect the assumed distribution of frictional parameters, $(a-b)\sigma_{\text{eff}}$: Red and blue colors denote stable ($(a-b)\sigma_{\text{eff}} > 0$) and

unstable ($(a - b)\sigma_{\text{eff}} < 0$) regions, respectively. The blue-colored region roughly corresponds to the depth of the source region with a large slip in simulated Nankai Trough megathrust earthquakes and is thus termed a “hyper-asperity.” In the hyper-asperity, we identify two segments with L values smaller than those of the other region (dark blue). The shallower one, identified at a depth of 10–11 km with a length along the plate boundary fault of 10 km (“shallower asperity” hereafter), causes M6 earthquakes. The deeper one is defined at a depth of 13–17 km, with a length of 30 km along the plate boundary fault (“deeper asperity” hereafter). The deeper asperity is set to model the high slip deficit rate patch deduced from the inversion analysis of the slip deficit rate distribution reported by Yokota et al. (2016) (Additional file 2: Figure S2). The slip deficit rate during the interseismic period may reflect a degree of interplate coupling. If so, parts with high slip deficit rate may release larger coseismic slip than parts with relatively low slip deficit rate. Such heterogeneity in the slip deficit rate (and possible resultant variation in the coseismic slip distribution) can be modeled by the heterogeneous distribution of L in the seismic cycle simulation with RSF. Under the constant $(a - b)\sigma_{\text{eff}}$ condition, small L values generate a higher slip deficit rate and a larger coseismic slip than large L values. Therefore, we assume a smaller L value at the deeper asperity than for the rest of the hyper-asperity (light-blue region). Similarly, the shallower asperity is also set to model the source of the off-Mie earthquake with a smaller L value.

As proposed by Hori and Miyazaki (2010, 2011), it is known that the existence of a smaller asperity, defined by a region with a much smaller L value relative to its surroundings, within the hyper-asperity tends to cause hierarchical rupture behavior. During the cycle of earthquakes rupturing the entire hyper-asperity, smaller earthquakes rupturing only the smaller asperity can occur without propagating to the surroundings. Accordingly, both shallower and deeper asperities with smaller L values in our model can produce the complex seismic cycle behavior of a hyper-asperity, depending on the assumed gap in L . Here, we simulate earthquake cycle scenarios primarily by modifying the gap in L values in the hyper-asperity so that the following two behaviors are satisfied: (i) M8-class earthquake that ruptures the hyper-asperity only occurs when the deeper asperity begins to rupture and (ii) the shallower asperity only ruptures a part of the hyper-asperity and its postseismic slip (afterslip/slow slip) mainly occurs at the shallow part of the shallower asperity.

To satisfy the latter constraint (ii), the shallow side of the plate interface must gradually reduce the slip deficit during an M8 earthquake cycle so that shear stress on the shallower asperity accumulates. To achieve this, we

first assumed that the shallowest interface (depth > 10 km) exhibits stable sliding with $(a - b)\sigma_{\text{eff}} > 0$; however, the stable sliding condition did not place a sufficient load on the shallower asperity to trigger an M6 earthquake. Therefore, we added the steady sliding zone at the top of the plate interface as a boundary condition (gray segment in Fig. 6a, depth from 5 to 6 km), where the plate interface was assumed to be slipping with a constant slip velocity of plate subduction V_{pl} . The application of this boundary condition is realized by excluding the upper-most sub-faults from the numerical computation, because our model only considers the perturbation from steady sliding on the plate interface.

After many trial simulations with the above boundary condition, we found that the frictional distribution shown in Fig. 6b provides the scenario most consistent with the above two constraints. In this study, we only present the scenario obtained for the frictional parameters shown in Fig. 6b, which has implications for the Nankai Trough megathrust earthquake cycles.

Additional files

Additional file 1: Figure S1. Names of DONET1 stations and nodes. Gray contours represent depth distribution of the top of oceanic crust layer 2 (Citak et al. 2012). (PDF 1118 kb)

Additional file 2: Figure S2. Comparison of hypocenter distribution with the slip deficit rate (SDR). Red circles represent hypocenters obtained in this study. SDR is after Yokota et al. (2016). (PDF 184 kb)

Additional file 3: Figure S3. A schematic image of 2.5-D velocity model used for hypocenter determination. (PDF 165 kb)

Additional file 4: Supplementary note. (DOCX 35 kb)

Additional file 5: Figure S4. Dependence of hypocenter locations on (a) stations used, (b) use of S-wave first arrivals, and (c) strike direction of PS plate. Values in brackets represent the RMS travel time residual. Plots are along the line A–B shown in Fig. 2a. (PDF 82 kb)

Abbreviations

CMT: Centroid moment tensor; DONET: Dense Oceanfloor Network System for Earthquakes and Tsunamis; MCS: Multi-channel seismic survey; OBS: Ocean-bottom seismometers; PSP: Philippine Sea plate; RMS: Root-mean-square; RSF: Rate- and state-dependent friction; SSE: Slow slip event; TOC: Top of the oceanic crust layer 2; TWT: Two-way travel time; VLFE: Very-low-frequency earthquake

Acknowledgements

We appreciate comments from Dr. L. Wallace and an anonymous reviewer, which greatly improved the manuscript. We also appreciate Dr. Y. Yamamoto for sharing data for plotting Fig. 2. The Japan Meteorological Agency unified earthquake catalogue was used to plot Fig. 1. All figures were drawn using Generic Mapping Tools (Wessel and Smith 1998).

Authors' contributions

MN conducted the hypocenter determinations and proposed the model. MH performed the numerical simulations of the hierarchical asperity model. MN and MH wrote the paper. AN and MY processed the structural data from MCS reflection surveys. TH and TT organized the geophysical interpretations. SKa and KS participated in the data processing for hypocenter determinations. SKo, NT, and YK organized the data acquisitions and the project. All authors equally contributed to scientific discussions. All authors read and approved the final manuscript.

Competing interests

The authors declare that they have no competing interests.

Publisher's Note

Springer Nature remains neutral with regard to jurisdictional claims in published maps and institutional affiliations.

Author details

¹R&D Center for Earthquake and Tsunami, Japan Agency for Marine-Earth Science and Technology, Yokohama, Japan. ²Earthquake and Volcano Research Unit, National Research Institute for Earth Science and Disaster Resilience, Tsukuba, Japan. ³Institute of Education, Research and Regional Cooperation for Crisis Management Shikoku, Kagawa University, Takamatsu, Japan.

Received: 28 December 2017 Accepted: 14 May 2018

Published online: 05 June 2018

References

- Akuhara T, Mochizuki K (2014) Application of cluster analysis based on waveform cross-correlation coefficients to data recorded by ocean-bottom seismometers: results from off the Kii Peninsula. *Earth Planets Space* 66:80. <https://doi.org/10.1186/1880-5981-66-80>.
- Akuhara T, Mochizuki K, Nakahigashi K, Yamada T, Shinohara M, Sakai S, Kanazawa T, Uehira K, Shimizu H (2013) Segmentation of the Vp/Vs ratio and low-frequency earthquake distribution around the fault boundary of the Tonankai and Nankai earthquakes. *Geophys Res Lett* 40:1306–1310. <https://doi.org/10.1002/grl.50223>.
- Ando M (1975) Source mechanisms and tectonic significance of historical earthquakes along the Nankai Trough, Japan. *Tectonophysics* 27:119–140.
- Annoura S, Hashimoto T, Kamaya N, Katsumata A (2017) Shallow episodic tremor near the Nankai Trough axis off southeast Mie prefecture, Japan. *Geophys Res Lett* 44:3564–3571. <https://doi.org/10.1002/2017GL073006>.
- Araki E, Saffer DM, Kopf AJ, Wallace LM, Kimura T, Machida Y, Ide S, Davis E, IODP Expedition 365 shipboard scientists (2017) Recurring and triggered slow-slip events near the trench at the Nankai Trough subduction megathrust. *Science* 356:1157–1160. <https://doi.org/10.1126/science.aan3120>.
- Ariyoshi K, Nakata R, Matsuzawa T, Hino R, Hori T, Hasegawa A, Kaneda Y (2014) The detectability of shallow slow earthquakes by the Dense Oceanfloor Network system for Earthquakes and Tsunamis (DONET) in Tonankai district, Japan. *Mar Geophys Res* 35:295–310. <https://doi.org/10.1007/s11001-013-9192-6>.
- Bangs NLB, Moore GF, Gulick SPS, Pangborn EM, Tobin HJ, Kuramoto S, Taira A (2009) Broad, weak regions of the Nankai Megathrust and implications for shallow coseismic slip. *Earth Planet Sci Lett* 284:44–49. <https://doi.org/10.1016/j.epsl.2009.04.026>.
- Bird P (2003) An updated digital model of plate boundaries. *Geochem Geophys Geosyst* 4:1027. <https://doi.org/10.1029/2001GC000252>.
- Citak SO, Nakamura T, Nakanishi A, Yamamoto Y, Ohori M, Baba T, Kaneda Y (2012) An updated model of three-dimensional seismic structure in the source area of the Tokai–Tonankai–Nankai earthquake. In abstract of AOGS–AGU (WPGM) Joint Assembly, Singapore, 13–17 august 2012, abstract no. OS06-A015.
- DeMets C, Gordon RG, Argus DF (2010) Geologically current plate motions. *Geophys J Int* 181:1–80. <https://doi.org/10.1111/j.1365-246X.2009.04491.x>.
- Furumura T, Hayakawa T, Nakamura M, Koketsu K, Baba T (2008) Development of long-period ground motions from the Nankai Trough, Japan, earthquakes: observations and computer simulation of the 1944 Tonankai (M_w 8.1) and the 2004 SE Off-Kii Peninsula (M_w 7.4) earthquakes. *Pure Appl Geophys* 165: 585–607. <https://doi.org/10.1007/s00024-008-0318-8>.
- Hori T (2006) Mechanisms of separation of rupture area and variation in time interval and size of great earthquakes along the Nankai Trough, southwest Japan. *J Earth Sim* 5:8–19.
- Hori T, Miyazaki S (2010) Hierarchical asperity model for multiscale characteristic earthquakes: a numerical study for the off Kamaishi earthquake sequence in the NE Japan subduction zone. *Geophys Res Lett* 37:L10304. <https://doi.org/10.1029/2010GL042669>.
- Hori T, Miyazaki S (2011) A possible mechanism of M9 earthquake generation cycles in the area of repeating M7–8 earthquakes surrounded by aseismic sliding. *Earth Planets Space* 63:773–777. <https://doi.org/10.5047/eps.2011.06.022>.
- Hori T, Miyazaki S, Mitsui N (2009) A model of earthquake-generation cycle with scale-dependent frictional property—preliminary results and research plan for a project of evaluation for coming Tokai, Tonankai, and Nankai earthquakes. *J Disaster Res* 4:111–117.
- Hyodo M, Hori T (2013) Re-examination of possible great interplate earthquake scenarios in the Nankai Trough, southwest Japan, based on recent findings and numerical simulations. *Tectonophysics* 600:175–186. <https://doi.org/10.1016/j.tecto.2013.02.038>.
- Ichinose GA, Thio HK, Somerville PG, Sato T, Ishii T (2003) Rupture process of the 1944 Tonankai earthquake (Ms 8.1) from the inversion of teleseismic and regional seismograms. *J Geophys Res* 108:2497. <https://doi.org/10.1029/2003JB002393>.
- Ishibashi K (2004) Status of historical seismology in Japan. *Ann Geophys* 47: 339–368.
- Kamei R, Pratt RG, Tsuji T (2012) Waveform tomography imaging of a megasplay fault system in the seismogenic Nankai subduction zone. *Earth Planet Sci Lett* 317–318:343–353. <https://doi.org/10.1016/j.epsl.2011.10.042>.
- Kamei R, Pratt RG, Tsuji T (2013) On acoustic waveform tomography of wide-angle OBS data—strategies for pre-conditioning and inversion. *Geophys J Int* 194:1250–1280. <https://doi.org/10.1093/gji/ggt165>.
- Kaneda Y, Kawaguchi K, Araki E, Matsumoto H, Nakamura T, Kamiya S, Ariyoshi K, Hori T, Baba T, Takahashi N (2015) Development and application of an advanced ocean floor network system for megathrust earthquakes and tsunamis. In: Favali P et al (eds) *Seafloor observatories*. Springer, Heidelberg, pp 643–662. https://doi.org/10.1007/978-3-642-11374-1_252.
- Kaneko L, Ide S, Nakano M (2018) Slow earthquakes in the microseism frequency band (0.1–1.0 Hz) off Kii Peninsula, Japan. *Geophys Res Lett* 45. <https://doi.org/10.1002/2017GL076773>.
- Kawaguchi K, Kaneko S, Nishida T, Komine T (2015) Construction of the DONET real-time seafloor observatory for earthquakes and tsunami monitoring. In: Favali P et al (eds) *Seafloor observatories*. Springer, Heidelberg, pp 211–228. https://doi.org/10.1007/978-3-642-11374-1_10.
- Kisslinger C, Jones LM (1991) Properties of aftershock sequences in southern California. *J Geophys Res* 96:11,947–11,958.
- Kodaira S, Hori T, Ito A, Miura S, Fujie G, Park J-O, Baba T, Sakaguchi H, Kaneda Y (2006) A cause of rupture segmentation and synchronization in the Nankai trough revealed by seismic imaging and numerical simulation. *J Geophys Res* 111:B09301. <https://doi.org/10.1029/2005JB004030>.
- Lomax A, Virieux J, Volant P, Berge C (2000) Probabilistic earthquake location in 3D and layered models: introduction of a Metropolis–Gibbs method and comparison with linear locations. In: Thurber CH, Rabinowitz N (eds) *Advances in seismic event location*, Kluwer, Amsterdam, The Netherlands, pp 101–134.
- Matsuzawa T, Hirose H, Shibasaki B, Obara K (2010) Modeling short- and long-term slow slip events in the seismic cycles of large subduction earthquakes. *J Geophys Res* 115:B12301. <https://doi.org/10.1029/2010JB007566>.
- Mikumo T, Miyatake T (1979) Earthquake sequences on a frictional fault model with non-uniform strengths and relaxation times. *Geophys J R Astr Soc* 59: 497–522.
- Mochizuki K, Fujie G, Sato T, Kasahara J, Hino R, Shinohara M, Suyehiro K (1998) Heterogeneous crustal structure across a seismic block boundary along the Nankai Trough. *Geophys Res Lett* 25:2301–2304.
- Mochizuki K, Nakahigashi K, Kuwano A, Yamada T, Shinohara M, Sakai S, Kanazawa T, Uehira K, Shimizu H (2010) Seismic characteristics around the fault segment boundary of historical great earthquakes along the Nankai Trough revealed by repeated long-term OBS observations. *Geophys Res Lett* 37:L09304. <https://doi.org/10.1029/2010GL042935>.
- Moore GF, Bangs NL, Taira A, Kuramoto S, Pangborn E, Tobin HJ (2007) Three-dimensional splay fault geometry and implications for tsunami generation. *Science* 318:1128–1131. <https://doi.org/10.1126/science.1147195>.
- Murotani S, Shimazaki K, Koketsu K (2015) Rupture process of the 1946 Nankai earthquake estimated using seismic waveforms and geodetic data. *J Geophys Res* 120:5677–5692. <https://doi.org/10.1002/2014JB011676>.
- Nakanishi A, Kodaira S, Miura S, Ito A, Sato T, Park J-O, Kido Y, Kaneda Y (2008) Detailed structural image around splay-fault branching in the Nankai subduction seismogenic zone: results from a high-density ocean bottom seismic survey. *J Geophys Res* 113:B03105. <https://doi.org/10.1029/2007JB004974>.
- Nakanishi A, Shiobara H, Hino R, Kodaira S, Kanazawa T, Shimamura H (1998) Detailed subduction structure across the eastern Nankai Trough obtained from ocean bottom seismographic profiles. *J Geophys Res* 103:27,151–27,168.

- Nakano M, Hori T, Araki E, Kodaira S, Ide S (2018) Shallow very-low-frequency earthquakes accompany slow slip events in the Nankai subduction zone. *Nat Commun* 9:984. <https://doi.org/10.1038/s41467-018-03431-5>.
- Nakano M, Nakamura T, Kamiya S, Kaneda Y (2014) Seismic activity beneath the Nankai trough revealed by DONET ocean-bottom observations. *Mar Geophys Res* 35:271–284. <https://doi.org/10.1007/s11001-013-9195-3>.
- Nakano M, Nakamura T, Kamiya S, Ohori M, Kaneda Y (2013) Intensive seismic activity around the Nankai trough revealed by DONET ocean-floor seismic observations. *Earth Planets Space* 65:5–15. <https://doi.org/10.5047/eps.2012.05.013>.
- Nakano M, Nakamura T, Kaneda Y (2015) Hypocenters in the Nankai Trough determined by using data from both ocean-bottom and land seismic networks and a 3D velocity structure model: implications for seismotectonic activity. *Bull Seism Soc Am* 105:1594–1605. <https://doi.org/10.1785/10120140309>.
- Noda H, Nakatani M, Hori T (2013) Large nucleation before large earthquakes is sometimes skipped due to cascade-up—implications from a rate and state simulation of faults with hierarchical asperities. *J Geophys Res* 118:2924–2952. <https://doi.org/10.1002/jgrb.50211>.
- Noda H, Nakatani M, Hori T (2014) Coseismic visibility of a small fragile patch involved in the rupture of a large patch—implications from fully dynamic rate-state earthquake sequence simulations producing variable manners of earthquake initiation. *Progress Earth Planetary Sci* 1:8. <https://doi.org/10.1186/2197-4284-1-8>.
- Obana K, Kodaira S (2009) Low-frequency tremors associated with reverse faults in a shallow accretionary prism. *Earth Planet Sci Lett* 287:168–174. <https://doi.org/10.1016/j.epsl.2009.08.005>.
- Obana K, Kodaira S, Kaneda Y (2004) Microseismicity around rupture area of the 1944 Tonankai earthquake from ocean bottom seismograph observations. *Earth Planet Sci Lett* 222:561–572. <https://doi.org/10.1016/j.epsl.2004.02.032>.
- Obana K, Kodaira S, Kaneda Y (2005) Seismicity in the incoming/subducting Philippine Sea plate off the Kii Peninsula, central Nankai trough. *J Geophys Res* 110:B11311. <https://doi.org/10.1029/2004JB003487>.
- Park J-O, Fujie G, Wijerathne L, Hori T, Kodaira S, Fukao Y, Moore GF, Bangs NL, Kuramoto S, Taira A (2010) A low-velocity zone with weak reflectivity along the Nankai subduction zone. *Geology* 38:283–286. <https://doi.org/10.1130/G30205.1>.
- Park J-O, Kodaira S (2012) Seismic reflection and bathymetric evidences for the Nankai earthquake rupture across a stable segment-boundary. *Earth Planets Space* 64:299–303. <https://doi.org/10.5047/eps.2011.10.006>.
- Park J-O, Moore GF, Tsuru T, Kodaira S, Kaneda Y (2003) A subducted oceanic ridge influencing the Nankai megathrust earthquake rupture. *Earth Planet Sci Lett* 217:77–84. [https://doi.org/10.1016/S0012-821X\(03\)00553-3](https://doi.org/10.1016/S0012-821X(03)00553-3).
- Park J-O, Tsuru T, Kodaira S, Cummins PR, Kaneda Y (2002) Splay fault branching along the Nankai subduction zone. *Science* 297:1157–1160. <https://doi.org/10.1126/science.1074111>.
- Podvin P, Lecomte I (1991) Finite difference computation of traveltimes in very contrasted velocity models: a massively parallel approach and its associated tools. *Geophys J Int* 105:271–284.
- Rani S, Singh SJ (1992) Static deformation of a uniform half-space due to a long dip-slip fault. *Geophys J Int* 109:469–476.
- Rice JR (1993) Spatio-temporal complexity of slip on a fault. *J Geophys Res* 98:9885–9907.
- Sakaguchi A, Chester F, Curewitz D, Fabbri O, Goldsby D, Kimura G, Li C-F, Masaki Y, Screation EJ, Tsutsumi A, Ujiie K, Yamaguchi A (2011) Seismic slip propagation to the updip end of plate boundary subduction interface faults: vitrinite reflectance geothermometry on Integrated Ocean Drilling Program NanTro SEIZE cores. *Geology* 39:395–398. <https://doi.org/10.1130/G31642.1>.
- Sakai S, Yamada T, Shinohara M, Hagiwara H, Kanazawa T, Obana K, Kodaira S, Kaneda Y (2005) Urgent aftershock observation of the 2004 off the Kii Peninsula earthquake using ocean bottom seismometers. *Earth Planets Space* 57:363–368.
- Seno T (2005) The September 5, 2004 off the Kii Peninsula earthquakes as a composition of bending and collision. *Earth Planets Space* 57:327–332.
- Takemura S, Shiomi K, Kimura T, Saito T (2016) Systematic difference between first-motion and waveform-inversion solutions for shallow offshore earthquakes due to a low-angle dipping slab. *Earth Planets Space* 68:149. <https://doi.org/10.1186/s40623-016-0527-9>.
- Takenaka H, Kennett BLN (1996) A 2.5-D time-domain elastodynamic equation for plane-wave incidence. *Geophys J Int* 125:F5–F9.
- Tobin H, Henry P, Vannucchi P, Screation E (2014) Subduction zones: structure and deformation history. In: Stein R et al (eds) *Developments in marine geology*. Elsevier BV, pp 599–640. <https://doi.org/10.1016/B978-0-444-62617-2.00020-7>.
- Tsuji T, Ashi J, Strasser M, Kimura G (2015) Identification of the static backstop and its influence on the evolution of the accretionary prism in the Nankai Trough. *Earth Planet Sci Lett* 431:15–25. <https://doi.org/10.1016/j.epsl.2015.09.011>.
- Tsuji T, Kamei R, Pratt RG (2014) Pore pressure distribution of a mega-splay fault system in the Nankai Trough subduction zone: insight into up-dip extent of the seismogenic zone. *Earth Planet Sci Lett* 396:165–178. <https://doi.org/10.1016/j.epsl.2014.04.011>.
- Tsuji T, Minato S, Kamei R, Tsuru T, Kimura G (2017) 3D geometry of a plate boundary fault related to the 2016 Off-Mie earthquake in the Nankai subduction zone, Japan. *Earth Planet Sci Lett* 478:234–244. <https://doi.org/10.1016/j.epsl.2017.08.041>.
- Tsuru T, Miura S, Park J-O, Ito A, Fujie G, Kaneda Y, No T, Katayama T, Kasahara J (2005) Variation of physical properties beneath a fault observed by a two-ship seismic survey off Southwest Japan. *J Geophys Res* 110:B05405. <https://doi.org/10.1029/2004JB003036>.
- Utsu T (1961) A statistical study on the occurrence of aftershocks. *Geophys Mag* 30:521–605.
- Wallace LM, Araki E, Saffer D, Wang X, Roesner A, Kopf A, Nakanishi A, Power W, Kobayashi R, Kinoshita C, Toczko S, Kimura T, Machida Y, Carr S (2016) Near-field observations of an offshore M_w 6.0 earthquake from an integrated seafloor and subseafloor monitoring network at the Nankai Trough, southwest Japan. *J Geophys Res* 121:8338–8351. <https://doi.org/10.1002/2016JB013417>.
- Wessel P, Smith WHF (1998) New, improved version of generic mapping tools released. *Eos* 79:579.
- Yamamoto Y, Takahashi T, Kaiho Y, Obana K, Nakanishi A, Kodaira S, Kaneda Y (2017) Seismic structure off the Kii Peninsula, Japan, deduced from passive- and active-source seismographic data. *Earth Planet Science Lett* 461:163–175. <https://doi.org/10.1016/j.epsl.2017.01.003>.
- Yokota Y, Ishikawa T, Watanabe S, Tashiro T, Asada A (2016) Seafloor geodetic constrains on interplate coupling of the Nankai Trough megathrust zone. *Nature* 534:374–377. <https://doi.org/10.1038/nature17632>.

Submit your manuscript to a SpringerOpen® journal and benefit from:

- Convenient online submission
- Rigorous peer review
- Open access: articles freely available online
- High visibility within the field
- Retaining the copyright to your article

Submit your next manuscript at ► springeropen.com